Monitoring the high-altitude cusp with the Low Energy Neutral Atom imager: Simultaneous observations from IMAGE and Polar

S. Taguchi,[1] S.-H. Chen,[2] M. R. Collier,[3] T. E. Moore,[3] M.-C. Fok,[3] K. Hosokawa,[1] and A. Nakao[1]

Received 15 February 2005; revised 24 August 2005; accepted 13 September 2005; published 3 December 2005.

[1] The Low Energy Neutral Atom (LENA) imager on the IMAGE spacecraft in the dayside magnetosphere can detect neutral particles that are emitted in the magnetosheath flow. During a period of dynamic pressure of 4–6 nPa and interplanetary magnetic field (IMF) B_z of −5 to 3 nT on 12 April 2001, LENA on IMAGE at (X_{GSM}, Y_{GSM}, Z_{GSM}) $\sim$ (4 R_E, 0 R_E, 6 R_E) observed significant emission in the direction of the high-latitude magnetosheath. Detailed analyses have revealed that the high-latitude sheath emission consists of two parts: the stable emission at the higher latitudes and the lower-latitude emission that occurs on and off. During the interval of this event, the Polar spacecraft was located at somewhat lower latitudes than IMAGE in similar noon meridian, and the plasma observations with the Thermal Ions Dynamic Experiment showed that the entry of the cusp ions happens in concurrence with the appearance of the lower-latitude LENA emission. This coincidence strongly suggests that the cusp ions flowing earthward charge exchange with the hydrogen exosphere. For the higher-latitude emission, its stability suggests that the source is associated with the structure persistently existing, which is consistent with the recent result showing that the sheath flow in the cusp indentation can create neutral atom emissions. Comparison of the LENA emission and ACE solar wind suggests that the lower-latitude LENA emission occurs during the southward tilting of dawnward IMF, indicating that this emission is associated with the earthward ion flux along the newly reconnected field lines. Hence this unique event for the simultaneous observations strongly suggests that LENA monitors the entry of the ions in the cusp, which is triggered by the southward tilting of the IMF, and that the significant flux of the cusp ion entry occurs equatorward of and separately from the cusp indentation.

Citation: Taguchi, S., S.-H. Chen, M. R. Collier, T. E. Moore, M.-C. Fok, K. Hosokawa, and A. Nakaso (2005), Monitoring the high-altitude cusp with the Low Energy Neutral Atom imager: Simultaneous observations from IMAGE and Polar, *J. Geophys. Res.*, *110*, A12204, doi:10.1029/2005JA011075.

1. Introduction

[2] In understanding mass and energy deposition in the magnetosphere and ionosphere from the solar wind, the position and motion of the polar cusp is of great importance. The effect of the solar wind on the polar cusp has been extensively examined at low altitudes using plasma observations from spacecraft [e.g., *Burch*, 1973; *Meng*, 1983; *Newell and Meng*, 1988], and from observations of auroral emission using optical ground-based techniques [e.g., *Sandholt et al.*, 1994, 1998]. Recent studies with the satellite-borne aurora imager have added new features to our understanding of the cusp for the northward interplanetary magnetic field (IMF) [*Milan et al.*, 2000; *Fuselier et al.*, 2002]. The characteristics of the low-altitude cusp are now well understood, including its temporal variations with a time resolution of several minutes.

[3] The effect of the solar wind on the polar cusp at altitudes of about 5 to 9 R_E has been examined in detail with the Polar spacecraft. *Zhou et al.* [2000] identified a significant number of polar cusp crossings, and clarified the characteristics of the position of the polar cusp, including its dependence on the solar wind. At these altitudes, the cusp region is larger than at the top of the ionosphere because of the magnetic field geometry. In addition, since the spacecraft moves more slowly here than in a low-altitude orbit, a typical cusp crossing at the altitude of Polar takes about 30 min [e.g., *Zhou et al.*, 2000], which is much longer than the crossing time at ionospheric height (1–2 min).

[4] At higher altitudes than Polar, the cusp observations have an even longer period. Hawkeye spacecraft, which can

[1]Department of Information and Communication Engineering, University of Electro-Communications, Tokyo, Japan.
[2]Universities Space Research Association, NASA Goddard Space Flight Center, Greenbelt, Maryland, USA.
[3]NASA Goddard Space Flight Center, Greenbelt, Maryland, USA.

0148-0227/05/2005JA011075$09.00

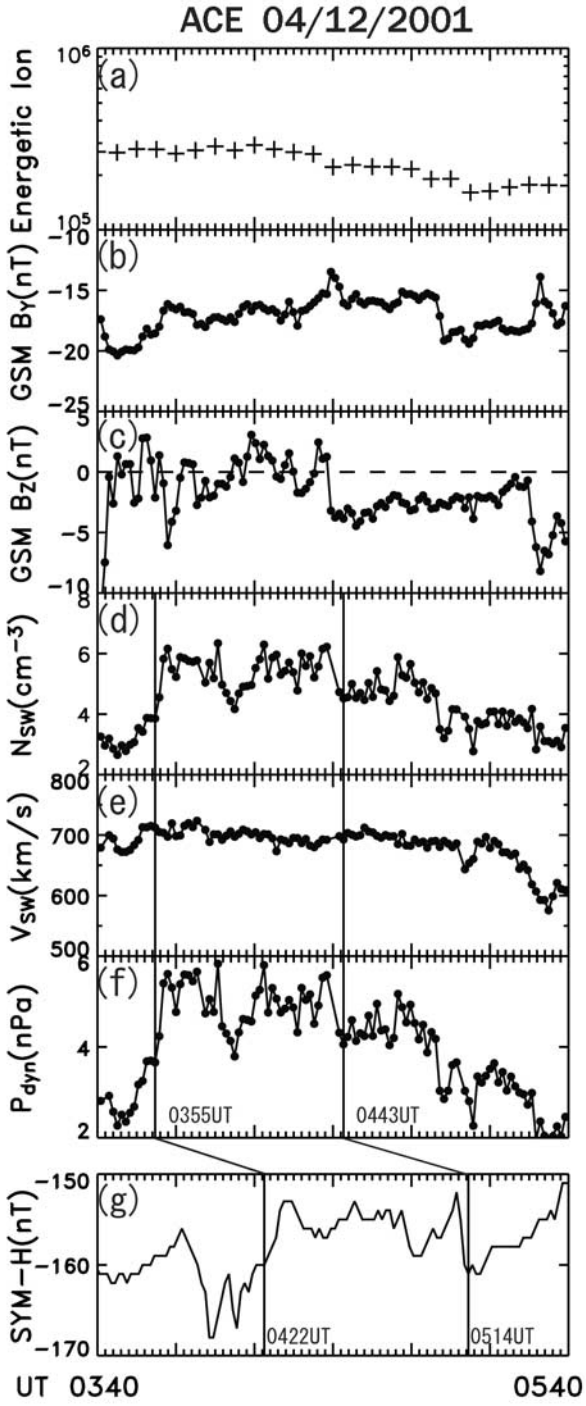

Figure 1. ACE solar wind data and SYM-H for the event in this study: (a) flux of energetic ions with energies between 47 and 65 keV el^{-1} (in units of counts s^{-1} cm^{-2} $ster^{-1}$ MeV^{-1}), (b) GSM Y component of the magnetic field, (c) GSM Z component, (d) solar wind number density, (e) GSM X component of velocity, (f) solar wind dynamic pressure, and (g) H component of the SYM index.

traverse at altitudes greater than 10 R_E, has revealed well-defined cusp crossings [e.g., *Farrell and Van Allen*, 1990]. The typical duration of these cusp crossings appears to be about 1 hour.

[5] It would seem that such long-duration cusp observations (~30 min to 1 hour), may exceed the several minute response time of the cusp to solar wind variations. In other words, results from analyses of the well-defined interval of the cusp crossing at such high altitudes reflect the cusp response to the solar wind for a timescale longer than ~30 min. To deduce the shorter timescale response, the field and plasma variations embedded in the large-scale structure must be examined as far as in situ spacecraft observations are concerned.

[6] Using Hawkeye data, *Chen et al.* [1997] presented an event identified in a possible location of the cusp indentation, and related the observed plasma and magnetic field variations, which had a timescale of several minutes, with the motion of the cusp as modulated by the varying IMF. Collection of this kind of event from in situ observations is expected to advance our understanding of the cusp dynamics at high altitudes. However, in using a single spacecraft it is difficult to find many cusp-crossing events that can be correlated with solar wind variations with a timescale of several minutes, because plasma and magnetic field data obtained in the cusp often include irregular or turbulent variations [*Dunlop et al.*, 2000].

[7] Recent remote sensing studies with the Low Energy Neutral Atom (LENA) imager [*Moore et al.*, 2000] on the IMAGE spacecraft have shed new light on the understanding of the dynamics of the high-altitude cusp. Extending the finding that neutral particles detected by LENA in the magnetosphere include the result of solar wind ions charge exchanging with the hydrogen exosphere in the magnetosheath flow [*Collier et al.*, 2001a, 2001b; *Fok et al.*, 2003; *Moore et al.*, 2003], *Taguchi et al.* [2004] have shown that the LENA emissions observed in the direction of the high-latitude magnetosheath during high dynamic pressures of ~20 nPa reflect the cusp indentation in the magnetopause shape, which suggests a means for monitoring the cusp motion using LENA.

[8] In this paper, we examine an IMAGE/LENA emission event for a period of moderately high dynamic pressure of 4–6 nPa on 12 April 2001. Results of analyses show that the LENA emission in the direction of the high-latitude sheath consists of two parts: the stable emission at the higher latitudes, and the lower-latitude emission that occurs on and off. We also show that appearance of the latter lower-latitude emission is consistent with the observation with the Thermal Ions Dynamic Experiment (TIDE) and the Magnetic Field Experiment (MFE) on the Polar spacecraft located somewhat at lower latitudes than IMAGE in the similar noon meridian. This consistency indicates that the entry of the cusp ions creates the LENA emissions, and that monitoring this entry with LENA is possible. Coupled with the existence of the emission at higher latitudes, which has been recently interpreted as the signal from the cusp indentation, we suggest that the significant flux of the cusp ion entry occurs equatorward of, and separately from the cusp indentation.

2. Solar Wind Conditions

[9] Figure 1 shows the solar wind conditions for the event that we analyzed in this study together with the SYM-H index. The ACE spacecraft was located about 200 R_E

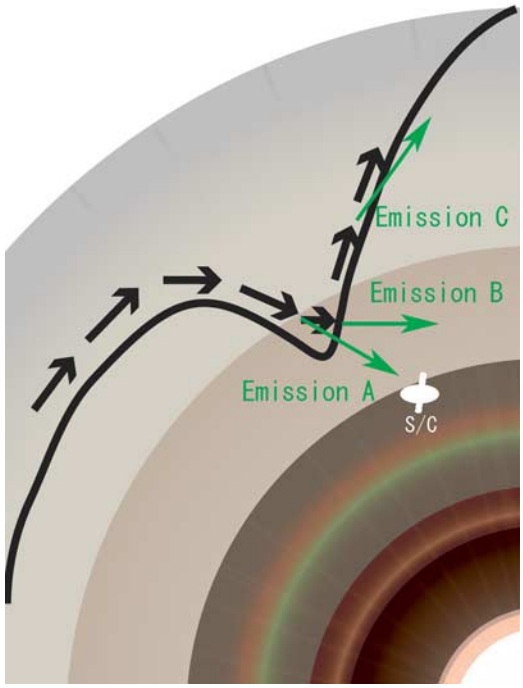

Figure 2. Schematic picture showing why the direction of the cusp indentation can be identified with IMAGE/LENA inside the magnetosphere. The bold curve represents the shape of the magnetopause that has the cusp indentation, and the sheath flow along the magnetopause is shown with the black arrows. The green arrows show the direction of possible neutral atom emission created in the cusp indentation.

upstream of the Earth. To check if energetic ions with energies of $\geq$50 keV el^{-1} (which is well above nominal upper limit on energy for LENA response) do not cause unexpected variation by penetrating the LENA collimator, we first examined solar wind ions with energies between 47 and 65 keV el^{-1} from the ACE Electron, Proton, and Alpha Monitor. The energetic ion data are plotted in Figure 1a. The variation is very gradual, which suggests that if the energetic ions penetrating the collimator cause LENA variation, it would be a relatively constant effect. In other words, if the LENA response varies with timescales much shorter than the very gradual variations of the solar wind energetic ions, it strongly suggests that the LENA response is not due to the energetic ions [*Collier et al.*, 2001a]. As is shown later, LENA observed emissions that occurs on and off with timescales of several minutes.

[10] Figures 1b and 1c show the IMF B_y and B_z, respectively, in GSM coordinates. We plotted 64-s averages of IMF data that were created from original 16-s averages so as to make comparison between the IMF and plasma data easier. During the plotted interval B_y is negative, and the dominant component. B_z varies mostly between ±3 nT in the first half of the interval, and becomes persistently negative after that. The B_x component varies mostly between ±5 nT through the interval (not shown).

[11] The solar wind dynamic pressure in Figure 1f was calculated from the density (Figure 1d) and speed (Figure 1e) assuming 4% He^{++} particles. Figure 1g shows the H component of the SYM index [*Iyemori and Rao*, 1996]. We related the start of a sharp increase of the solar wind dynamic pressure at 0355 UT (left line in Figures 1d, 1e, and 1f) and a decrease at 0443 UT (right line) with a positive sudden impulse (SI^+) at 0422 UT and a negative sudden impulse (SI^-) [*Araki and Nagano*, 1988; *Takeuchi et al.*, 2002] at 0514 UT, respectively. The time lag from ACE to Earth is then estimated to be 27–31 min.

3. Emission Observed by IMAGE/LENA

[12] Figure 2 illustrates where is the suitable position for monitoring the cusp indentation. When the sheath ion flow comes to the cusp indentation, neutral hydrogen can be emitted if there is adequate charge exchanging of ions with the hydrogen exosphere which is illustrated with several concentric circles. These circles simply represent that the exospheric neutral hydrogen densities are spherically symmetric [*Wallace et al.*, 1970; *Rairden et al.*, 1986], and their color does not reflect any density profiles. Note, however, that a slight asymmetry exists in the actual density profiles [*Østgaard et al.*, 2003].

[13] For simplicity, only three representative directions of the possible emission are shown (green arrows). When the spacecraft is situated as is shown in Figure 2, the spacecraft would observe clearly neutral hydrogen emitted in the direction of the arrow shown as Emission A. A simple model by *Taguchi et al.* [2004, Figure 5] shows that this kind of emission can be observed as a distinct peak in the distribution of the hydrogen count.

[14] For remote sensing of the cusp indentation, it is important that the emission does not overlap with neutral atoms coming directly from the Sun, because this flux, which is called the Sun signal [e.g., *Moore et al.*, 2001; *Collier et al.*, 2001a, 2003], is stronger than the emission in the direction of the cusp indentation. Emission B can be parallel to the Sun-Earth line, and would overlap the Sun signal when the spacecraft is located downstream of Emission B. Emission C can also overlap stronger emission when the spacecraft is located downstream of Emission C. The stronger emission may come from the magnetosheath near the equatorial plane [*Collier et al.*, 2005; *Taguchi et al.*, 2004]. Hence a spacecraft residing at a somewhat smaller Z than the possible location of the indentation would be suitable for monitoring the cusp.

[15] The sheath flow may slow down when it intrudes into the cusp indentation. This possible slowdown is favorable for LENA's cusp monitoring because there is a high probability that the flow in the cusp will stay within the nominal energy upper limit for the response of LENA to ions (converted negative ions) that the incident neutrals become by picking up an electron from the conversion surface inside LENA.

[16] Neutral atoms from the sheath would include components having higher energies than the nominal energy upper limit for the response of LENA. Since such energetic neutral atoms can cause "sputtering" of negative ions from the conversion surface of LENA, the negative ions, which have much lower energies than the incident neutrals, can be detected inside LENA [*Collier et al.*, 2001a]. For this reason, LENA can respond to incident neutrals with energies of up to at least 3–4 keV [*Moore et al.*, 2003], and cover the high-energy component of the sheath ions. This capability would

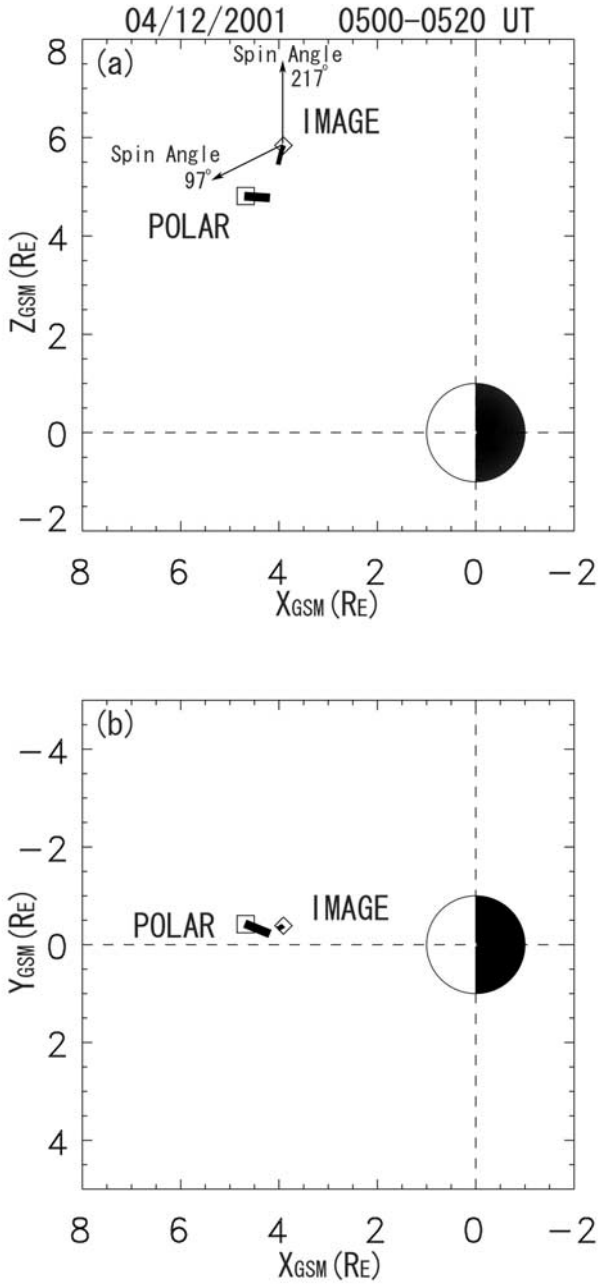

Figure 3. Position of IMAGE and Polar in (a) GSM *x-z* and (b) *x-y* planes for 12 April 2001, 0500–0520 UT. The squares indicate the location of the spacecraft at 0500 UT, and the short black lines from the squares represent the motion of the spacecraft during 0500–0520 UT. Two arrows from a point on the IMAGE orbit represent a 120° (217° minus 97°) field of view of LENA that is used for our analysis.

make the angular dispersion of the sputtered ions broader than the incident signal. Hence we did not examine the detail of spatial broadening of the incident signals, but analyzed the signals by focusing on the location of the peak count in a LENA snapshot.

[17] Figures 3a and 3b show the IMAGE orbit in the $X_{GSM} - Z_{GSM}$ and $X_{GSM} - Y_{GSM}$ planes for the interval that we analyzed in this paper, respectively. IMAGE is located near (X_{GSM}, Z_{GSM}) $\sim$ (4 R_E, 6 R_E) in the midnoon sector ($Y_{GSM} = -0.5$ R_E). Polar is located at somewhat lower latitudes than IMAGE, and in similar noon meridian plane.

[18] In Figure 3a, two arrows from the starting location on the IMAGE orbit indicate the approximate projection of a 120° field of view of LENA to the $Y_{GSM} = 0$ meridian. The upward arrow indicates the upper boundary of the 120°, which was decided as an 8° bin whose line of sight (LOS) makes the minimum angle from the *z* axis [*Taguchi et al.*, 2004]. The other arrow represents the lower boundary, which corresponds to the 8° bin that covers from 97° to 105°. This bin is three sectors (24°) from the solar direction.

[19] Figure 4 shows an example of the LENA snapshots obtained during the orbit shown in Figure 3. The background-corrected scaled hydrogen count rates observed at 0508 UT (which covers 0507 to 0509 UT) are plotted in the format of spin angle versus polar angle. The Sun signal is seen at lower spin angles. The details of the cause of the Sun signal have been reported by *Collier et al.* [2003, 2001a, 2001b]. Weak emission can be seen at the spin angles much larger than those of the Sun signal. This signal has been interpreted as being created in the cusp indentation [*Taguchi et al.*, 2004], and is referred to as the cusp indentation signal.

[20] Three images of Figure 5 show the same image as the one in Figure 4 plus two snapshots obtained 2 min before and after. The format of each plot of Figure 5 is the GSM *Z* versus *Y,* and the values of *Y* along the horizontal axis decrease from left to right, that is, from the postnoon to the prenoon side. The hydrogen count rate for each LOS is plotted at the (Y_{GSM}, Z_{GSM}) position of the intersection of a sphere surface with a radius of 8 R_E.

[21] The outer boundary shown with the white rectangle of Figure 4 is drawn in Figure 5 as a distorted boundary.

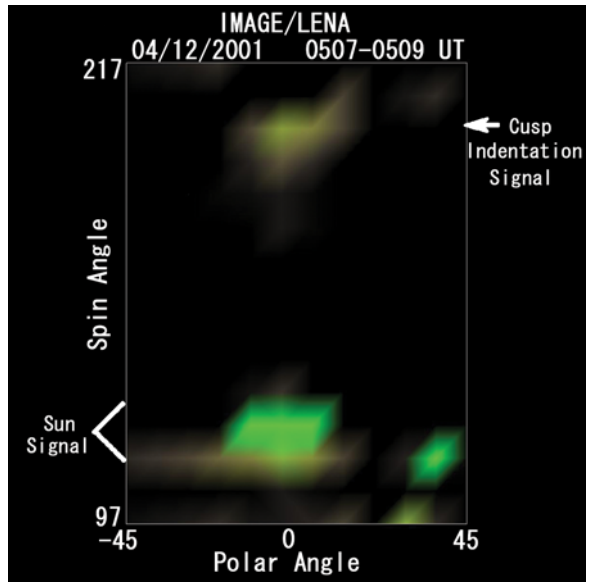

Figure 4. LENA snapshot obtained around 0508 UT on 12 April 2001. Background-corrected scaled hydrogen count rates are plotted in the format of the spin angle versus the Polar angle. The cusp indentation signal and the Sun signal can be seen.

The region inside the distorted white boundary in Figure 5 is somewhat narrow near $Z_{GSM} \sim 6.5\ R_E$ compared with the upper and lower parts. This simply reflects that the mapping surface for the field of view in the middle part is somewhat close to the location of the spacecraft. Note that the narrowest part in the middle is not any indication of the cusp indentation structure.

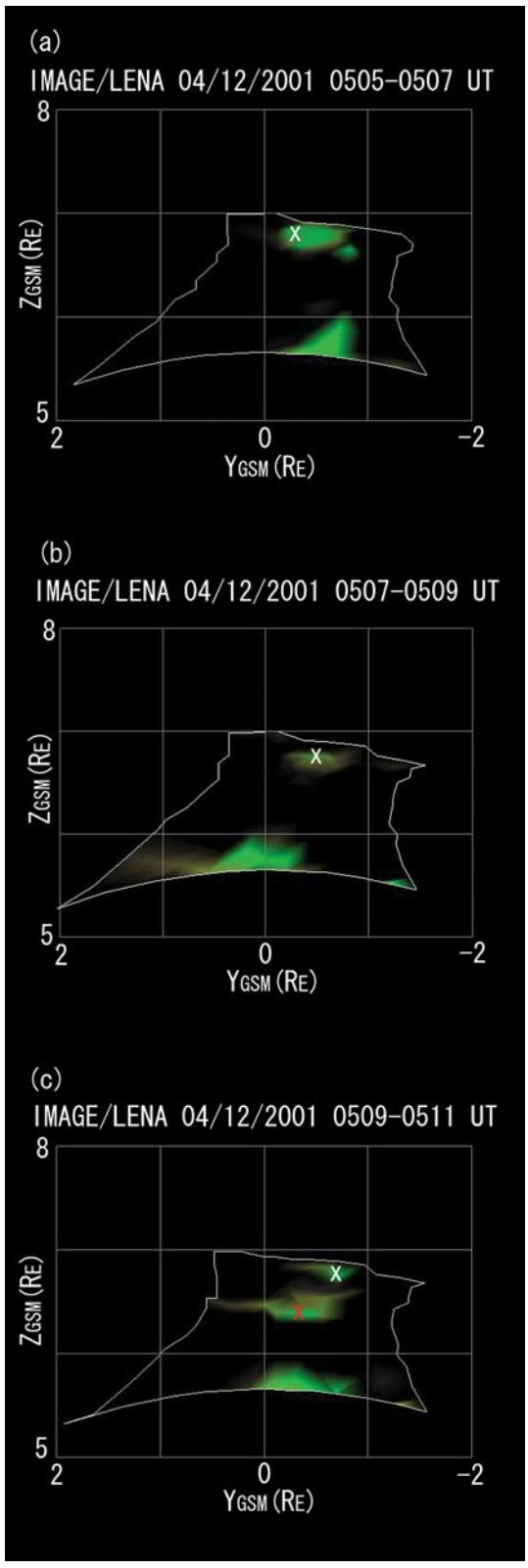

[22] In all snapshots of Figure 5 the Sun signal appears at $Z = 5\ R_E$ to $6\ R_E$. That emission should be seen in the Z position that is similar to the one for the spacecraft (Figure 3a) because it should come roughly along the x axis. At $Z = 6.5\ R_E$ to $7\ R_E$ in each plot there is another stable emission, that is, the cusp indentation signal. The peak of this emission is indicated with the white cross mark. For Figure 5b, the position of this peak on the sphere is (X_{GSM}, Y_{GSM}, Z_{GSM}) = (4.2 R_E, −0.5 R_E, 6.8 R_E).

[23] The field mapping based on the Tsyganenko 96 model shows that the northern ionospheric footprint is at a latitude of ~72.5° in corrected geomagnetic latitudes. This latitude is not inconsistent with the interpretation that the emission is the cusp indentation signal, although the input values of the IMF B_y (−15 nT) and *Dst* (−164 nT) for the Tsyganenko 96 model are beyond the range of reliable approximation. We note, however, that the latitude of ~72.5° is lower than the average of the cusp latitude for small IMF $|B_z|$ conditions [*Newell et al.*, 1989; *Taguchi et al.*, 1993].

[24] When Figure 5c is compared with Figures 5a and 5b, it is clear that emissions appear around $Z = 6.4\ R_E$ (indicated with the red cross), that is, equatorward of the cusp indentation signal. We will show in the next section that this emission is in concurrence with the entry of the cusp ions at Polar.

4. IMAGE/LENA and Polar/TIDE Observations

[25] The IMAGE/LENA and Polar observations for 0500–0520 UT, which include the above timing of the appearance of the LENA emission around $Z = 6.4\ R_E$ (Figure 5c), are shown in Figure 6. Figures 6a–6d show data from the Polar magnetic field experiment (MFE) [*Russell et al.*, 1995]. Figures 6e and 6f represent the TIDE spectrogram in spin angle versus UT and the one in energy versus UT, respectively. In Figure 6e, the minuses (pluses) indicate the direction (opposite direction) of the magnetic field projected on the spin plane with respect to the spacecraft moving direction indicated by the crosses (immediately below the minuses). If TIDE measures fluxes in the plus direction which is oriented in the opposite direction of the magnetic field, it means that the entry of the ions occurs in parallel with the magnetic field.

[26] TIDE can observe cold ions in the energy range 0.3 to 450 eV above the spacecraft potential during the 6-s spin period of the satellite [*Moore et al.*, 1995]. We used STOPS component in TIDE data, which gives collapsed three dimensional measurements as 2D velocity distributions in the spin plane, because the STARTS component, which

Figure 5. LENA image mapped on a sphere surface with a radius of 8 R_E for (a) 0505–0507 UT, (b) 0507–0509 UT, and (c) 0509–0511 UT. The hydrogen count rate for each line of sight is plotted at the (Y_{GSM}, Z_{GSM}) position of the intersection on the sphere. The count rate data in Figure 5b are the same as those for Figure 4. The white cross shows the location of the peak emission occurring at higher latitudes, that is, the cusp indentation signal. The red cross in Figure 5c indicates the peak of the signal at lower latitudes.

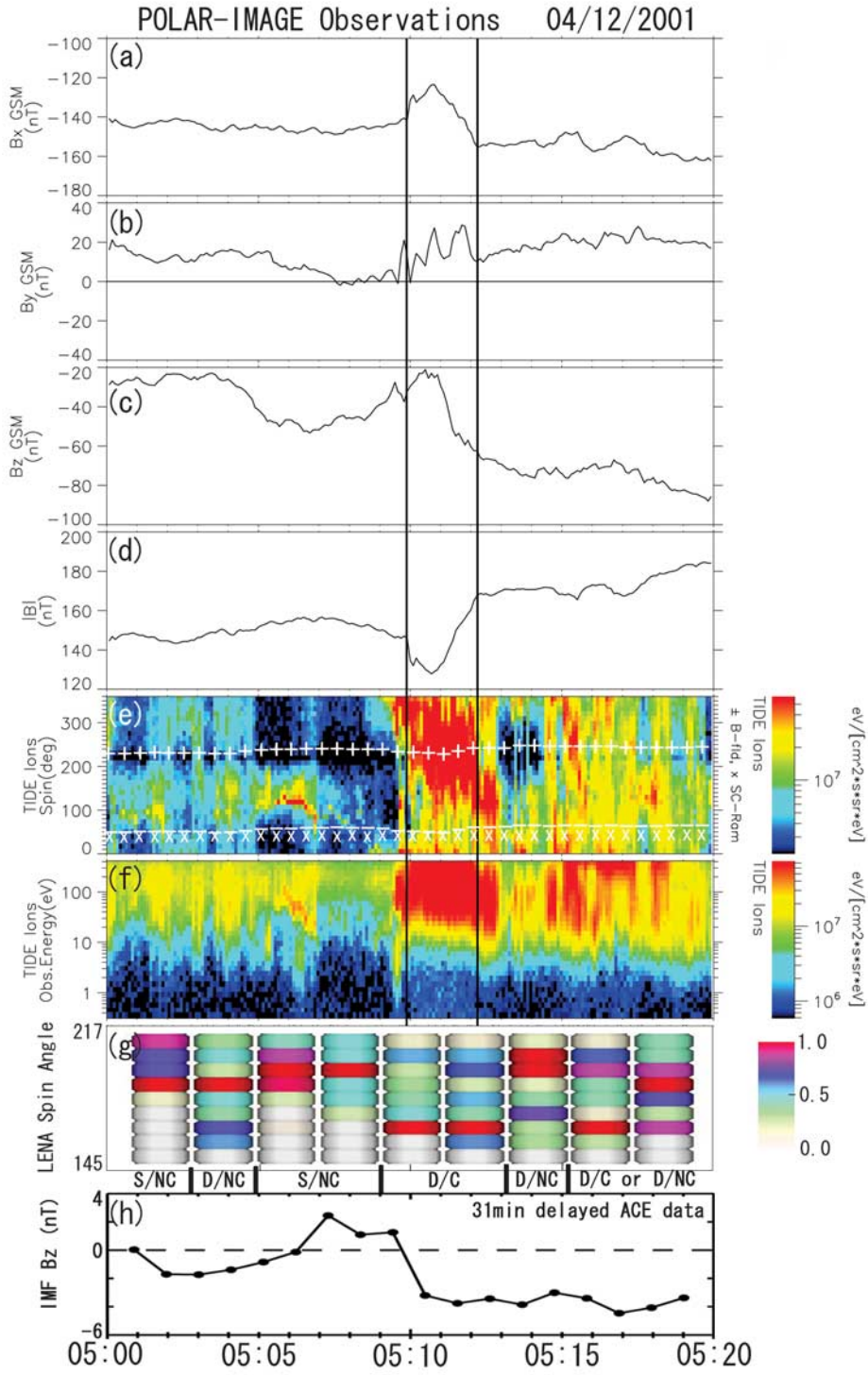

Figure 6. Comparison between (a–f) Polar, (g) IMAGE/LENA, and (h) ACE observations during the period 0500–0520 UT. Magnetic field data obtained by Polar are shown in Figures 6a–6d. Figure 6e is the spectrogram in the spin angle versus UT, and Figure 6f is the one in the format of energy versus UT. In Figure 6e, the pluses (minuses) indicate the direction (opposite direction) of the magnetic field projected on the spin plane with respect to the spacecraft moving direction indicated by the crosses. They also indicate parallel (antiparallel) flows along the plus (minus) direction. Figure 6g shows the LENA normalized counts in each time and range bin. Red indicates the spin angle for the maximum count in each time. The two vertical lines represent the interval of the cusp ion entry observations, which is determined with the magnetic field depression and the higher energy flux of the ions. Figure 6h shows the IMF B_z variations observed by ACE.

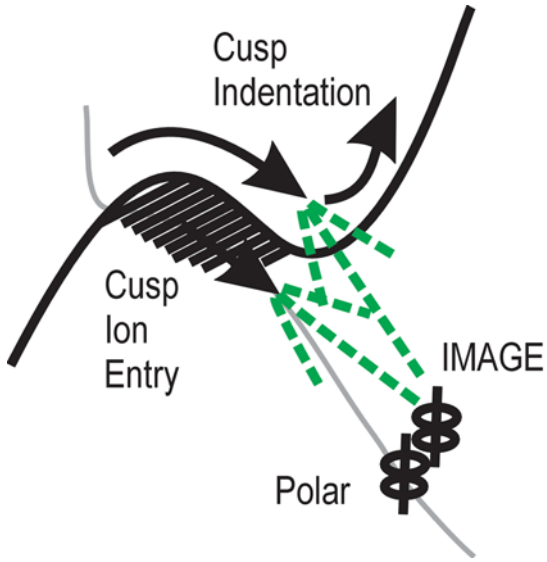

Figure 7. Schematic illustration of the interpretation of the simultaneous observations from IMAGE/LENA and Polar/TIDE around 0510 UT on 12 April 2001. The solid arrow in the hatched region represents the flow of the ion entry, and the curved arrows in the indentation show the sheath plasma flow. The dashed green lines from the arrows represent the emission of the neutral atoms. The longest green line from the black arrow represents the emission that reaches the position of IMAGE.

provides 3D measurements, was not functioning after late 1996 [*Chen and Moore*, 2004].

[27] Figure 6g shows a LENA spectrogram for spin angles of 145°–217°. This range does not include the Sun signal. Counts are normalized so that the maximum peak of the hydrogen background-corrected scaled count rate can be unity in each time and spin angle range [*Taguchi et al.*, 2004]. At 0509 UT the maximum count (red region) shifted to smaller angles, that is, to the third bin from the bottom, while keeping a minor peak (blue color) at higher angles. In other words, the distribution becomes a double peak structure (Figure 5c).

[28] This timing is concurrent with the Polar/TIDE observations of the significant ion flux, which are shown in Figures 6e and 6f. Before ~0509:30 UT the energy flux at Polar is relatively low, indicating the tenuous magnetospheric population. After that, the higher energy flux is observed in concurrence with the depression of the total magnetic field (Figure 6d), that is, the entry of the cusp ions is identified. The left vertical line (at 0510 UT) indicates the time when the depression of the magnetic field starts. The maximum depression occurs around 0511 UT, and the decrease of $|B|$ from 0510 to 0511 UT is about 20 nT. Around 0512:10 UT the magnetic field returns the background level. This time is shown with the right vertical line.

[29] The ion distribution at a period between the two lines (Figure 6e) has a field-aligned flow, that is, the entry of the ions along the magnetic field as far as it is observed with a low-energy instrument, TIDE. From the concurrence of the cusp ion entry at Polar/TIDE with the appearance of the LENA emission at the smaller angle bins at 0509–0513 UT (Figure 6g), it is strongly suggested that the cusp ion entry creates the neutral atom emission through charge exchanging with hydrogen exosphere.

[30] After that, Polar entered the magnetospheric population (0513–0515 UT). Then it again observed relatively high energy flux in concurrence with the small depression of the total magnetic field at 0515–0516 and 0517–0518 UT. From these multiple occurrences of the cusp-like properties, it seems that the cusp observation around 0510 UT is not the traversal of the stationary whole cusp structure. Rather, it would be related to some temporal change, for example, the motion of the region of the ion entry. We note that the encounter of the cusp ion entry in the present observation is short when compared with the typical cusp crossing at the altitude of Polar, that is, about 30 min [e.g., *Zhou et al.*, 2000].

[31] We show simple categorization of the LENA and TIDE observations below Figure 6g. In this categorization S or D before the slash means that the LENA emission is single or double, respectively. The letter after the slash, C or NC represents whether Polar observed the cusp ion entry or the noncusp, respectively.

[32] As mentioned above, Polar appears to be in the cusp-like population after 0515 UT. However, since the energy flux is somewhat lower and the magnetic depression is smaller during such a period of time than during 0510–0512 UT when the typical cusp ion entry occurs, it is hard to tell unambiguously whether the region is a part of the cusp or not. We have just shown this situation as "D/C or D/NC." During such an interval the LENA emission has a double structure. The LENA double emission can be also seen at 0503–0505 UT. During this interval, Polar was in the magnetospheric population, that is, the noncusp.

[33] Figure 6h shows 31-min delayed ACE B_z data. This time delay comes from the estimation made in Figure 1. It is clear that the appearance of the LENA lower-latitude emission at 0509 UT is in concurrence with the negative change of the IMF B_z, and that the double emission continues during the interval of the negative IMF B_z. The agreement between the double emission and the negative B_z can be also seen around 0504 UT. Hence the appearance of the lower-latitude emission, which is concurrent with the significant flux of the cusp ions at Polar, is associated with the southward tilting of IMF.

5. Discussion and Conclusions

[34] When IMF B_z is negative, reconnection occurs on the dayside magnetopause. Newly reconnected flux tubes pass through the cusp entry layer, where the ions move earthward along the magnetic field lines. These ions would produce neutral atoms when they reach the place where the hydrogen density in the exosphere is adequate. This situation is schematically shown in Figure 7.

[35] The hatched region in Figure 7 represents the region where the entry of ions occurs, that is, the plasma entry layer [*Paschmann et al.*, 1976] or the interior cusp [*Chen et al.*, 1997]. The arrow from this shaded region shows the ion entry along the magnetic field line (gray line). This line represents an open field line after the reconnection.

[36] Green dashed lines from the magnetic filed line (gray) represent neutral atom emissions. Some of these emissions can reach the position of IMAGE, and this type

of emission is identified as the lower-latitude part of the emissions. The higher-latitude part of the emissions is shown with the dashed green lines from the cusp indentation. This kind of emissions is caused by the sheath ion flow, that is, Emission A in Figure 2. Hence our interpretation suggests that the cusp ion entry is operative equatorward of and separately from the cusp indentation.

[37] We examine below if it is possible for the cusp ion entry to produce observable counts of the neutral atom emissions. From the TIDE plasma moments for 0–400 eV, the number density and velocity around 0512 UT are calculated to be 12 cm^{-3} and 38 km s^{-1}, respectively (not shown). The number flux for this energy range is 4.6×10^7 cm^{-2} s^{-1}. For the cusp ions, there should be a hotter component above 400 eV. To obtain the total flux, we need to include this contribution, and multiply the flux by a factor of $1 \sim 2$. For example, when we take 1.5 for the factor, the ion total flux is $\sim 7 \times 10^7$ cm^{-2} s^{-1}.

[38] For simplicity, we regard the charge exchange of the ions as being operative between the altitude of IMAGE (at $R \sim 7\ R_E$) and $R = 10\ R_E$. The latter value reflects the distance of the model magnetopause [*Shue et al.*, 1998] in the direction of the LENA peak emission for the corresponding solar wind conditions, that is, $B_z = 0$ nT, and $P_{dyn} = 5$ nPa. When the LENA's field of view for a single spin sector falls in the region of the source ion flux, the neutral atom flux, Φ_N obtained at that spin angle is expressed as the integral of the ion flux Φ_{ION}, multiplied by the charge exchange cross section σ and the hydrogen exospheric density, n_H along the line of sight [*Collier et al.*, 2001b; *Taguchi et al.*, 2004, and references therein]. When we assume that the line of sight is along the radial direction from the center of the Earth, and that σ and Φ_{ION} (7×10^7 cm^{-2} s^{-1}) does not vary along the line of sight from $R = 7\ R_E$ to $R = 10\ R_E$, Φ_N can be estimated as

$$\Phi_N = \Phi_{ION}\sigma \int_{7R_E}^{10R_E} n_H dR. \quad (1)$$

[39] Using the recent result for the neutral hydrogen density by *Østgaard et al.* [2003, Figure 10], we can calculate the above integral from $R = 7\ R_E$ to $R = 10\ R_E$ to be $\sim 5 \times 10^{10}$ cm^{-2}. Taking $\sigma \sim 2 \times 10^{-15}$ cm^2 [*Gealy and Van Zyl*, 1987; *Collier et al.*, 2005], we get $\Phi_N \sim 7 \times 10^3$ cm^{-2} s^{-1}. When we take 1.9×10^{-4} for LENA's neutral hydrogen detection efficiency for the time period of the present observation, Φ_N of 7×10^3 cm^{-2} s^{-1} would correspond to a count rate of 1.3 s^{-1} at LENA whose entrance aperture has an area of 1 cm^2. Since each spin sector is observed for about 2.7 s, this count rate would be about 4 count per spin. It thus appears that the cusp ion entry produces neutral atom emissions that can be detected by LENA, although this count is somewhat lower than the actual observation, 12 count/spin in the sector for the peak of the lower-latitude emission (Figure 5c).

[40] In Figure 6 we have shown that the lower-latitude emission continues after 0509 UT. This suggests that the ion entry occurs continuously. On the other hand, the Polar observations show that the ion entry disappears for a while after 0513 UT. From these facts, we know that the disappearance of the ion entry at Polar is due to the exit of Polar from the region of the cusp ion entry, not due to the stop of the ion entry. The reason for this interpretation is that the LENA lower-latitude peak (purple color) at 0513–0515 UT occurs at one bin larger angle than before, that is, the source moves poleward. For the double emission at 0503–0505 UT (Figure 6), there are no corresponding signatures at Polar. This indicates that Polar was still located well equatorward of the cusp entry region at that time.

[41] In conclusion, the simultaneous observations from IMAGE/LENA and Polar/TIDE have shown that the LENA emission in the direction of the high-latitude magnetosheath consists of two parts, and that the lower-latitude emission can occur in concurrence with the entry of the cusp ions at Polar located at somewhat lower latitudes than IMAGE in similar noon meridian. This concurrence can be interpreted as the charge exchange of the earthward flowing cusp ions with the hydrogen exosphere. This kind of neutral atom emission seems to happen during the southward tilting of IMF, suggesting that the cusp ions for this emission occur on the newly reconnected field lines. The higher-latitude emission is stable, and operative separately from the lower-latitude emission. Its stability suggests that the source is associated with the structure persistently existing, which is consistent with the recent result showing that the sheath flow in the cusp indentation can create neutral atom emissions. These observations suggest that LENA can monitor the entry of the cusp ions, and that the significant flux of the ion entry occurs equatorward of, and separately from the cusp indentation.

[42] **Acknowledgments.** The initial part of this study was made while S. Taguchi was at the Universities Space Research Association, NASA/GSFC, during his sabbatical from the University of Electro-Communications, Japan. S.-H. Chen's work was supported by the Polar mission under UPN 370-08-43. This research was supported by the IMAGE project under UPN 370-28-20 at the Goddard Space Flight Center and by grant-in-aid 15540427 in category C under the Japan Society for the Promotion of Science. Special thanks go to Atsushi Yamazaki for his help in the interpretation. Polar magnetic field data and ACE solar wind data are provided by NASA/NSSDC. The authors thank C. T. Russell (PI of Polar magnetic field data), D. McComas (PI of ACE plasma data), N. Ness (PI of ACE magnetic field data), and R. Gold (PI of ACE EPAM data). We also thank WDC for Geomagnetism, Kyoto, Japan, for providing the midlatitude SYM-H index.

[43] Lou-Chuang Lee thanks Mark Lester and Nikolai Ostgaard for their assistance in evaluating this paper.

References

Araki, T., and H. Nagano (1988), Geomagnetic response to sudden expansions of the magnetosphere, *J. Geophys. Res.*, *93*, 3983–3988.

Burch, J. L. (1973), Rate of erosion of the dayside magnetic flux based on a quantitative study of the dependence of Polar cusp latitude on the interplanetary magnetic field, *Radio Sci.*, *8*, 955.

Chen, S.-H., and T. E. Moore (2004), Dayside flow bursts in the Earth's outer magnetosphere, *J. Geophys. Res.*, *109*, A03215, doi:10.1029/2003JA010007.

Chen, S.-H., S. A. Boardsen, S. F. Fung, J. L. Green, R. L. Kessel, L. C. Tan, T. E. Eastman, and J. D. Craven (1997), Exterior and interior Polar cusps: Observations from Hawkeye, *J. Geophys. Res.*, *102*, 11,335–11,347.

Collier, M. R., et al. (2001a), Observations of neutral atoms from the solar wind, *J. Geophys. Res.*, *106*, 24,893–24,906.

Collier, M. R., et al. (2001b), LENA observations on March 31, 2001: Magnetosheath remote sensing, *Eos Trans. AGU*, *82*(47), Fall Meet. Suppl., Abstract SM41C-05.

Collier, M. R., et al. (2003), Dust in the wind: The dust geometric cross section at 1 AU based on neutral solar wind observations, in *Solar Wind 10: Proceedings of the Tenth International Solar Wind Conference*, edited by M. Velli, R. Bruno, and F. Malara, *AIP Conf. Proc.*, *679*, 790–793.

Collier, M. R., T. E. Moore, M.-C. Fok, B. Pilkerton, and S. Boardsen (2005), Low-energy neutral atom signatures of magnetopause motion

in response to southward B_z, *J. Geophys. Res.*, *110*, A02102, doi:10.1029/2004JA010626.

Dunlop, M. W., P. J. Cargill, T. J. Stubbs, and P. Woolliams (2000), The high-altitude cusps: HEOS 2, *J. Geophys. Res.*, *105*, 27,509–27,517.

Farrell, W. M., and J. A. Van Allen (1990), Observations of the Earth's polar cleft at large radial distances with the Hawkeye 1 magnetometer, *J. Geophys. Res.*, *95*, 20,945–20,958.

Fok, M.-C., et al. (2003), Global ENA IMAGE simulations, *Space Sci. Rev.*, *109*, 77–103.

Fuselier, S. A., H. U. Frey, K. J. Trattner, S. B. Mende, and J. L. Burch (2002), Cusp aurora dependence on interplanetary magnetic field B_z, *J. Geophys. Res.*, *107*(A7), 1111, doi:10.1029/2001JA900165.

Gealy, M. W., and B. Van Zyl (1987), Cross sections for electron capture and loss. I. H^+ and H^- impact on H and H_2, *Phys. Rev. A*, *36*, 3091–3099.

Iyemori, T., and D. R. K. Rao (1996), Decay of the *Dst* component of geomagnetic disturbance after substorm onset and its implication to storm substorm relation, *Ann. Geophys.*, *14*, 608–618.

Milan, S. E., M. Lester, S. W. H. Cowley, and M. Brittnacher (2000), Dayside convection and auroral morphology during an interval of northward interplanetary magnetic field, *Ann. Geophys.*, *18*, 436–444.

Meng, C.-I. (1983), Case studies of the storm time variations of the polar cusp, *J. Geophys. Res.*, *88*, 137–149.

Moore, T. E., et al. (1995), The thermal ion dynamics experiment and plasma source instrument, *Space Sci. Rev.*, *71*, 409.

Moore, T. E., et al. (2000), The low-energy neutral atom imager for IMAGE, *Space Sci. Rev.*, *91*, 155–195.

Moore, T. E., et al. (2001), Low energy neutral atoms in the magnetosphere, *Geophys. Res. Lett.*, *28*, 1143–1146.

Moore, T. E., M. R. Collier, M.-C. Fok, S. A. Fuselier, H. Khan, W. Lennartsson, D. G. Simpson, G. R. Wilson, and M. O. Chandler (2003), Heliosphere-geosphere interactions using low energy neutral atom imaging, *Space Sci. Rev.*, *109*, 351–371.

Newell, P. T., and C.-I. Meng (1988), The cusp and cleft/boundary: Low altitude identification and statistical local time variations, *J. Geophys. Res.*, *93*, 14,549–14,556.

Newell, P. T., C.-I. Meng, D. G. Sibeck, and R. P. Lepping (1989), Some low-altitude cusp dependencies on interplanetary magnetic field, *J. Geophys. Res.*, *94*, 8921–8927.

Østgaard, N., S. B. Mende, H. U. Frey, G. R. Gladstone, and H. Lauche (2003), Neutral hydrogen density profiles derived from geocoronal imaging, *J. Geophys. Res.*, *108*(A7), 1300, doi:10.1029/2002JA009749.

Paschmann, G., G. Haerendel, N. Sckopke, and H. Rosenbauer (1976), Plasma and magnetic field characteristics of the distant polar cusp near local noon: The entry layer, *J. Geophys. Res.*, *81*, 2883–2899.

Rairden, R. L., L. A. Frank, and J. D. Craven (1986), Geocoronal imaging with Dynamics Explorer, *J. Geophys. Res.*, *91*, 13,613–13,630.

Russell, C. T., R. C. Snare, J. D. Means, D. Pierce, D. Dearborn, M. Larson, G. Barr, and G. Le (1995), The GGS POLAR magnetic fields investigation, *Space Sci. Rev.*, *71*, 563–582.

Sandholt, P. E., et al. (1994), Cusp/cleft auroral activity in relation to solar wind dynamic pressure, interplanetary magnetic field B_z, and B_y, *J. Geophys. Res.*, *99*, 17,323–17,342.

Sandholt, P. E., C. J. Farrugia, M. Øieroset, P. Stauning, and W. F. Denig (1998), Auroral activity associated with unsteady magnetospheric erosion: Observations on December 18, 1990, *J. Geophys. Res.*, *103*, 2309–2318.

Shue, J.-H., et al. (1998), Magnetopause location under extreme solar wind conditions, *J. Geophys. Res.*, *103*, 17,691–17,700.

Taguchi, S., M. Sugiura, J. D. Winningham, and J. A. Slavin (1993), Characterization of the IMF B_y-dependent field-aligned currents in the cleft region based on DE 2 observations, *J. Geophys. Res.*, *98*, 1393–1407.

Taguchi, S., M. R. Collier, T. E. Moore, M.-C. Fok, and H. J. Singer (2004), Response of neutral atom emissions in the low-latitude and high-latitude magnetosheath direction to the magnetopause motion under extreme solar wind conditions, *J. Geophys. Res.*, *109*, A04208, doi:10.1029/2003JA010147.

Takeuchi, T., T. Araki, A. Viljanen, and J. Watermann (2002), Geomagnetic negative sudden impulses: Interplanetary causes and polarization distribution, *J. Geophys. Res.*, *107*(A7), 1096, doi:10.1029/2001JA900152.

Wallace, L., C. A. Barth, J. B. Pearce, K. K. Kelly, D. E. Anderson Jr., and W. G. Fastie (1970), Mariner 5 measurement of the Earth's Lyman alpha emission, *J. Geophys. Res.*, *75*, 3769–3777.

Zhou, X. W., C. T. Russell, G. Le, S. A. Fuselier, and J. D. Scudder (2000), Solar wind control of the polar cusp at high altitude, *J. Geophys. Res.*, *105*, 245–251.

S.-H. Chen, Universities Space Research Association, NASA Goddard Space Flight Center, Greenbelt, MD 20771, USA.

M. R. Collier, M.-C. Fok, and T. E. Moore, NASA Goddard Space Flight Center, Greenbelt, MD 20771, USA.

K. Hosokawa, A. Nakao, and S. Taguchi, Department of Information and Communication Engineering, University of Electro-Communications, Chofu, Tokyo, 182-8585, Japan. (taguchi@ice.uec.ac.jp)